

Positive-parity excited states of the nucleon in quenched lattice QCDM. S. Mahbub,^{1,2} Alan Ó. Cais,^{1,3} Waseem Kamleh,¹ Derek B. Leinweber,¹ and Anthony G. Williams¹¹*Special Research Centre for the Subatomic Structure of Matter, Adelaide, South Australia 5005, Australia, and Department of Physics, University of Adelaide, South Australia 5005, Australia*²*Department of Physics, Rajshahi University, Rajshahi 6205, Bangladesh*³*Cyprus Institute, Guy Ourisson Building, Athalassa Campus, PO Box 27456, 1645 Nicosia, Cyprus*
(Received 3 May 2010; revised manuscript received 2 September 2010; published 8 November 2010)

Positive-parity spin- $\frac{1}{2}$ excitations of the nucleon are explored in lattice QCD. The variational method is used in this investigation and several correlation matrices are employed. As our focus is on the utility and methodology of the variational approach, we work in the quenched approximation to QCD. Various sweeps of Gaussian fermion-field smearing are applied at the source and at the sink of $\chi_1\bar{\chi}_1$ and $\chi_1\chi_2$ correlation functions to obtain a large basis of operators. Using several different approaches for constructing basis interpolators, we demonstrate how improving the basis can split what otherwise might be interpreted as a single state into multiple eigenstates. Consistency of the extracted excited energy states are explored over various dimensions of the correlation matrices. The use of large correlation matrices is emphasized for the reliable extraction of the excited eigenstates of QCD.

DOI: [10.1103/PhysRevD.82.094504](https://doi.org/10.1103/PhysRevD.82.094504)

PACS numbers: 11.15.Ha, 12.38.-t, 12.38.Gc

I. INTRODUCTION

One of the long-standing puzzles in hadron spectroscopy has been the low mass of the first positive parity, $J^P = \frac{1}{2}^+$, excitation of the nucleon, known as the Roper resonance $N^*(1440 \text{ MeV})$. In constituent or valence quark models with harmonic oscillator potentials, the lowest-lying odd parity state naturally occurs below the $N = \frac{1}{2}^+$ state (with principal quantum number $N = 2$) [1,2] whereas, in Nature the Roper resonance is almost 100 MeV below the $N = \frac{1}{2}^-$ (1535 MeV) state. Similar difficulties in the level orderings appear for the $J^P = \frac{3}{2}^+ \Delta^*(1600)$ and $\frac{1}{2}^+ \Sigma^*(1690)$ resonances, which have led to the speculation that the Roper resonance may be more appropriately viewed as a hybrid baryon state with explicitly excited glue field configurations [3,4] or as a breathing mode of the ground state [5] or states which can be described in terms of meson-baryon dynamics alone [6].

Lattice QCD is very successful in computing many properties of hadrons from first principles. In particular, in hadron spectroscopy, the ground states of the hadron spectrum are now well understood [7]. However, the excited states still prove a significant challenge as they belong to the subleading exponential of the two-point correlation function. Extracting excited-states masses from these subleading exponents is difficult as the correlation functions decay quickly and the signal-to-noise ratio deteriorates more rapidly. In baryon spectroscopy, there are many experimentally observed baryon resonances whose physical properties are poorly understood. Lattice QCD can provide theoretical input to solidify their identification. The first detailed analysis of the positive-parity excitation of the nucleon was performed in Ref. [8] using Wilson fermions and an operator product expansion spectral ansatz. Since then several attempts have been made to

address these issues in the lattice framework [9–20], but in many cases no potential identification of the Roper state has been made. Recently, however, in the analysis of Refs. [14,15,21] a low-lying Roper state has been identified using Bayesian techniques.

Another state-of-the-art approach in hadron spectroscopy is the “variational method” [22,23], which is based on a correlation matrix analysis. The identification of the Roper state with this method have been mixed. However, recently, in Ref. [24] a low-lying Roper state has been identified with this approach employing a diverse range of smeared-smeared correlation functions. Our work there motivates us to investigate the several positive-parity excited states using similar techniques but in a significantly more comprehensive manner.

In this paper, the variational analysis used in Refs. [24,25] is explored more extensively. In particular, we consider 6×6 and 8×8 correlation matrices not only built from the χ_1 interpolating field, but also incorporating another nucleon interpolator, χ_2 , to extend the set of basis operators. 6×6 matrices are built up using $\chi_1\bar{\chi}_1$ and $\chi_1\chi_2$ correlators, while the 8×8 matrices use the $\chi_1\chi_2$ correlation functions, as discussed in the text.

One of the goals of this paper is to investigate the high-lying positive-parity spin- $\frac{1}{2}$ excited states of the nucleon, such as $P_{11}(1710 \text{ MeV})$ and $P_{11}(2100 \text{ MeV})$, using larger correlation matrices. Incorporating the χ_2 interpolator with various numbers of smearing sweeps enables us to explore more deeply the overlapping of different interpolators with the energy eigenstates. This will also prove the reliability of the discovery of the Roper resonance [24]. We demonstrate how improving the basis interpolating fields can split what otherwise might be interpreted as a single state into multiple eigenstates.

This paper is arranged as follows: Sec. II contains the general description of the extraction of masses with the introduction of different nucleon interpolating fields. The lattice details are given in Sec. III, the results are presented in Sec. IV, and conclusions are made in Sec. V.

II. MASS OF HADRONS

The masses of hadrons are extracted from two-point correlation functions using operators chosen to have overlap with desired states. Let us consider a baryon state B of spin half, if we suppress Dirac indices a two-point function can be written as

$$G_{ij}(t, \vec{p}) = \sum_{\vec{x}} e^{-i\vec{p}\cdot\vec{x}} \langle \Omega | T \{ \chi_i(x) \bar{\chi}_j(0) \} | \Omega \rangle. \quad (1)$$

The operator $\bar{\chi}_j(0)$ creates states from the vacuum at space-time point 0 and, following the evolution of the states in time t , the states are destroyed by the operator $\chi_i(x)$ at point \vec{x} , t . T stands for the time-ordered product of operators. A complete set of momentum eigenstates provides

$$\sum_{B, \vec{p}', s} |B, \vec{p}', s\rangle \langle B, \vec{p}', s| = I, \quad (2)$$

where B can include multiparticle states. The substitution of Eq. (2) into Eq. (1) yields

$$G_{ij}(t, \vec{p}) = \sum_{\vec{x}} \sum_{B, \vec{p}', s} e^{-i\vec{p}\cdot\vec{x}} \langle \Omega | \chi_i(x) | B, \vec{p}', s \rangle \times \langle B, \vec{p}', s | \bar{\chi}_j(0) | \Omega \rangle. \quad (3)$$

We can express the operator $\chi_i(x)$ as

$$\chi_i(x) = e^{iP \cdot x} \chi_i(0) e^{-iP \cdot x}, \quad (4)$$

where, $P^\mu = P = (H, \vec{P})$ and \vec{P} is the momentum operator whose eigenvalue is the total momentum of the system. Equation (3) can now be written as,

$$\begin{aligned} G_{ij}(t, \vec{p}) &= \sum_{\vec{x}} \sum_{B, \vec{p}', s} e^{-i\vec{p}\cdot\vec{x}} \langle \Omega | e^{iP \cdot x} \chi_i(0) e^{-iP \cdot x} | B, \vec{p}', s \rangle \\ &\times \langle B, \vec{p}', s | \bar{\chi}_j(0) | \Omega \rangle \\ &= \sum_{\vec{x}} \sum_{B, \vec{p}', s} e^{-iE_B t} e^{-i\vec{x}\cdot(\vec{p}-\vec{p}')} \langle \Omega | \chi_i(0) | B, \vec{p}', s \rangle \\ &\times \langle B, \vec{p}', s | \bar{\chi}_j(0) | \Omega \rangle. \end{aligned} \quad (5)$$

As we move from Minkowski space to Euclidean space, the time $t \rightarrow -it$ and the above equation then can be written as

$$\begin{aligned} G_{ij}(t, \vec{p}) &= \sum_{B, \vec{p}', s} e^{-E_B t} \delta_{\vec{p}, \vec{p}'} \langle \Omega | \chi_i(0) | B, \vec{p}', s \rangle \\ &\times \langle B, \vec{p}', s | \bar{\chi}_j(0) | \Omega \rangle \\ &= \sum_B \sum_s e^{-E_B t} \langle \Omega | \chi_i(0) | B, \vec{p}, s \rangle \langle B, \vec{p}, s | \bar{\chi}_j(0) | \Omega \rangle. \end{aligned} \quad (6)$$

The overlap of the interpolating fields $\chi(0)$ and $\bar{\chi}(0)$ with positive and negative parity baryon states $|B^\pm\rangle$ can be parametrized by a complex quantity called the coupling strength, λ_{B^\pm} , which can be defined for positive-parity states by

$$\langle \Omega | \chi(0) | B^+, \vec{p}, s \rangle = \lambda_{B^+} \sqrt{\frac{M_{B^+}}{E_{B^+}}} u_{B^+}(\vec{p}, s), \quad (7)$$

$$\langle B^+, \vec{p}, s | \bar{\chi}(0) | \Omega \rangle = \bar{\lambda}_{B^+} \sqrt{\frac{M_{B^+}}{E_{B^+}}} \bar{u}_{B^+}(\vec{p}, s). \quad (8)$$

For the negative parity states one requires

$$\langle \Omega | \chi(0) | B^-, \vec{p}, s \rangle = \lambda_{B^-} \sqrt{\frac{M_{B^-}}{E_{B^-}}} \gamma_5 u_{B^-}(\vec{p}, s), \quad (9)$$

$$\langle B^-, \vec{p}, s | \bar{\chi}(0) | \Omega \rangle = -\bar{\lambda}_{B^-} \sqrt{\frac{M_{B^-}}{E_{B^-}}} \bar{u}_{B^-}(\vec{p}, s) \gamma_5. \quad (10)$$

Here, λ_{B^\pm} and $\bar{\lambda}_{B^\pm}$ are the couplings of the interpolating functions at the sink and the source, respectively, and M_{B^\pm} is the mass of the state B^\pm . E_{B^\pm} is the energy of the state B^\pm , where $E_{B^\pm} = \sqrt{M_{B^\pm}^2 + \vec{p}^2}$, and $u_{B^\pm}(\vec{p}, s)$ and $\bar{u}_{B^\pm}(\vec{p}, s)$ are the Dirac spinors,

$$\bar{u}_{B^\pm}^\alpha(\vec{p}, s) u_{B^\pm}^\beta(\vec{p}, s) = \delta^{\alpha\beta}. \quad (11)$$

Thus, Eq. (6) contains a projection operator $\Gamma_\pm = \sum_s u_{B^\pm}^\beta(\vec{p}, s) \bar{u}_{B^\pm}^\alpha(\vec{p}, s)$, through which the contributions to the even and odd parity states from the correlation function can be obtained. For positive parity, this can be expressed as

$$\sum_s u_{B^+}^\beta(\vec{p}, s) \bar{u}_{B^+}^\alpha(\vec{p}, s) = \frac{\gamma \cdot p + M_{B^+}}{2E_{B^+}}, \quad (12)$$

and for the negative parity,

$$\gamma_5 \left(\sum_s u_{B^-}^\beta(\vec{p}, s) \bar{u}_{B^-}^\alpha(\vec{p}, s) \right) \gamma_5 = \frac{-\gamma \cdot p + M_{B^-}}{2E_{B^-}}. \quad (13)$$

By substituting the above equations, for the positive and negative parity states in Eq. (6) we obtain

$$\begin{aligned} G_{ij}(t, \vec{p}) &= \sum_{B^+} \lambda_{B^+} \bar{\lambda}_{B^+} e^{-E_{B^+} t} \frac{\gamma \cdot p_{B^+} + M_{B^+}}{2E_{B^+}} \\ &+ \sum_{B^-} \lambda_{B^-} \bar{\lambda}_{B^-} e^{-E_{B^-} t} \frac{-\gamma \cdot p_{B^-} + M_{B^-}}{2E_{B^-}}. \end{aligned} \quad (14)$$

At momentum $\vec{p} = \vec{0}$, $E_{B^\pm} = M_{B^\pm}$, a parity projection operator Γ_\pm can be introduced,

$$\Gamma_\pm = \frac{1}{2} (1 \pm \gamma_0). \quad (15)$$

We can isolate the masses of the even and odd parity states by taking the trace of \mathcal{G} with the operators Γ_+ and Γ_- . The positive-parity state propagates through the (1,1) and (2,2)

elements of the Dirac matrix, whereas, the negative parity state propagates through the (3,3) and (4,4) elements.

The correlation function for positive and negative parity states can then be written as

$$G_{ij}^{\pm}(t, \vec{0}) = \text{Tr}_{\text{sp}}[\Gamma_{\pm} \mathcal{G}_{ij}(t, \vec{0})] = \sum_{B^{\pm}} \lambda_i^{\pm} \bar{\lambda}_j^{\pm} e^{-M_{B^{\pm}} t}. \quad (16)$$

The correlation function contains a superposition of states. The mass of the lowest state, $M_{0^{\pm}}$ can be extracted at large t where the contributions from all other states are suppressed,

$$G_{ij}^{\pm}(t, \vec{0}) \xrightarrow{t \rightarrow \infty} \lambda_{i0}^{\pm} \bar{\lambda}_{j0}^{\pm} e^{-M_{0^{\pm}} t}. \quad (17)$$

A. Source smearing

The spatial source smearing [26] technique is applied to increase the overlap of the interpolators with the lower-lying states. We employ a fixed boundary condition in the time direction for the fermions by setting $U_i(\vec{x}, N_t) = 0 \forall \vec{x}$ in the hopping terms of the fermion action with periodic boundary conditions imposed in the spatial directions. Gauge invariant Gaussian smearing [26] in the spatial dimensions is applied through an iterative process. The smearing procedure is

$$\psi_i(x, t) = \sum_{x'} F(x, x') \psi_{i-1}(x', t), \quad (18)$$

where

$$F(x, x') = (1 - \alpha) \delta_{x, x'} + \frac{\alpha}{6} \sum_{\mu=1}^3 [U_{\mu}(x) \delta_{x', x+\hat{\mu}} + U_{\mu}^{\dagger}(x - \hat{\mu}) \delta_{x', x-\hat{\mu}}], \quad (19)$$

where the parameter $\alpha = 0.7$ is used in our calculation. After repeating the procedures N_{sm} times on a point source the resulting smeared fermion field is

$$\psi_{N_{\text{sm}}}(x, t) = \sum_{x'} F^{N_{\text{sm}}}(x, x') \psi_0(x', t). \quad (20)$$

B. Variational method

The extraction of the ground state mass can be done straightforwardly. However access to the excited state masses requires additional effort. Here we consider the variational method [22,23]. The variational method requires the cross correlation of operators so that the operator space can be diagonalized and the excited state masses extracted from the exponential nature of the diagonalized basis. To access N states of the spectrum, one requires a minimum of N interpolators. With the assumption that only N states contribute significantly to G_{ij} at time t , the parity projected two-point correlation function matrix for $\vec{p} = 0$ can be written as

$$G_{ij}^{\pm}(t) = \left(\sum_{\vec{x}} \text{Tr}_{\text{sp}} \{ \Gamma_{\pm} \langle \Omega | \chi_i(x) \bar{\chi}_j(0) | \Omega \rangle \} \right) \quad (21)$$

$$= \sum_{\alpha=0}^{N-1} \lambda_i^{\alpha} \bar{\lambda}_j^{\alpha} e^{-m_{\alpha} t}, \quad (22)$$

where Dirac indices are implicit. Here, λ_i^{α} and $\bar{\lambda}_j^{\alpha}$ are the couplings of interpolators χ_i and $\bar{\chi}_j$ at the sink and source, respectively, to eigenstates $\alpha = 0, \dots, (N-1)$. m_{α} is the mass of the state α . The N interpolators have the same quantum numbers and provide an N -dimensional basis upon which to describe the states. Using this basis we aim to construct N independent interpolating source and sink fields which isolate N baryon states $|B_{\alpha}\rangle$, i.e.

$$\bar{\phi}^{\alpha} = \sum_{i=1}^N u_i^{\alpha} \bar{\chi}_i, \quad (23)$$

$$\phi^{\alpha} = \sum_{i=1}^N v_i^{\alpha} \chi_i, \quad (24)$$

such that,

$$\langle B_{\beta}, p, s | \bar{\phi}^{\alpha} | \Omega \rangle = \delta_{\alpha\beta} \bar{z}^{\alpha} \bar{u}(\alpha, p, s), \quad (25)$$

$$\langle \Omega | \phi^{\alpha} | B_{\beta}, p, s \rangle = \delta_{\alpha\beta} z^{\alpha} u(\alpha, p, s), \quad (26)$$

where z^{α} and \bar{z}^{α} are the coupling strengths of ϕ^{α} and $\bar{\phi}^{\alpha}$ to the state $|B_{\alpha}\rangle$. Consider a real eigenvector u_j^{α} which operates on the correlation matrix $G_{ij}(t)$ from the right, one can obtain [12],

$$G_{ij}(t) u_j^{\alpha} = \left(\sum_{\vec{x}} \text{Tr}_{\text{sp}} \{ \Gamma_{\pm} \langle \Omega | \chi_i \bar{\chi}_j | \Omega \rangle \} \right) u_j^{\alpha} = \lambda_i^{\alpha} \bar{z}^{\alpha} e^{-m_{\alpha} t}. \quad (27)$$

For notational convenience, in the remainder of the discussion the repeated indices i, j, k are to be understood as being summed over, whereas, α , which stands for a particular state, is not. Since the only t dependence comes from the exponential term, we can write a recurrence relation at time $(t + \Delta t)$ as,

$$G_{ij}(t + \Delta t) u_j^{\alpha} = e^{-m_{\alpha} \Delta t} G_{ij}(t) u_j^{\alpha}, \quad (28)$$

for sufficiently large t and $t + \Delta t$ [25,27].

Multiplying the above equation by $[G_{ij}(t)]^{-1}$ from the left we get,

$$[(G(t))^{-1} G(t + \Delta t)] u^{\alpha} = e^{-m_{\alpha} \Delta t} u^{\alpha} = c^{\alpha} u^{\alpha}. \quad (29)$$

This is an eigenvalue equation for eigenvector u^{α} with eigenvalue $c^{\alpha} = e^{-m_{\alpha} \Delta t}$. We can also solve the left eigenvalue equation to recover the v^{α} eigenvector,

$$v_i^{\alpha} G_{ij}(t + \Delta t) = e^{-m_{\alpha} \Delta t} v_i^{\alpha} G_{ij}(t). \quad (30)$$

Similarly,

$$v^\alpha[G(t + \Delta t)(G(t))^{-1}] = e^{-m_a \Delta t} v^\alpha. \quad (31)$$

The vectors u_j^α and v_i^α diagonalize the correlation matrix at time t and $t + \Delta t$ making the projected correlation matrix,

$$v_i^\alpha G_{ij}(t) u_j^\beta = \delta^{\alpha\beta} z^\alpha \bar{z}^\beta e^{-m_a t}. \quad (32)$$

The parity projected, eigenstate projected correlator, $v_i^\alpha G_{ij}^\pm(t) u_j^\alpha \equiv G_\pm^\alpha$ is then used to obtain masses of different states. We construct the effective mass

$$M_{\text{eff}}^\alpha(t) = \ln\left(\frac{G_\pm^\alpha(t, \vec{0})}{G_\pm^\alpha(t + 1, \vec{0})}\right) = M_\pm^\alpha, \quad (33)$$

and apply standardized analysis techniques as described in Ref. [25].

III. SIMULATION DETAILS

We use an ensemble of 200 quenched configurations with a lattice volume of $16^3 \times 32$. Gauge field configurations are generated by using the doubly blocked Wilson action in two coupling space (DBW2) [28,29]. An $\mathcal{O}(a)$ -improved fat link irrelevant clover (FLIC) fermion action [30] is used to generate quark propagators. This action has excellent scaling properties and provides near continuum results at finite lattice spacing [31]. The lattice spacing is $a = 0.127$ fm, as determined by the static quark potential, with the scale set with the Sommer scale, $r_o = 0.49$ fm [32]. In the irrelevant operators of the fermion action we apply four sweeps of stout-link smearing to the gauge links to reduce the coupling with the high frequency modes of the theory [33]. We use the same method as in Ref. [34] to determine fixed boundary effects, and the effects are significant only after time slice 25 in the present analysis.

Eight different levels of gauge invariant Gaussian smearing [26] (1, 3, 7, 12, 16, 26, 35, 48 sweeps corresponding to rms radii, in lattice units, of 0.6897, 1.0459, 1.5831, 2.0639, 2.3792, 3.0284, 3.5237, 4.1868) are applied at the source (at $t = 4$) and at the sink. This is to ensure a variety of overlaps of the interpolators with the lower-lying states. The analysis is performed on nine different quark masses providing pion masses of $m_\pi = \{0.797, 0.729, 0.641, 0.541, 0.430, 0.380, 0.327, 0.295, 0.249\}$ GeV. The error analysis is performed using the jackknife method, where the χ^2/dof is obtained via a covariance matrix analysis method.

The nucleon interpolators we consider in this analysis are

$$\chi_1(x) = \epsilon^{abc}(u^{Ta}(x)C\gamma_5 d^b(x))u^c(x), \quad (34)$$

$$\chi_2(x) = \epsilon^{abc}(u^{Ta}(x)Cd^b(x))\gamma_5 u^c(x). \quad (35)$$

We use the Dirac representation of the gamma matrices in our analysis.

Each of the 6×6 correlation matrices of $\chi_1 \bar{\chi}_1$ correlators corresponds to a particular selection of 6 levels of smearing from the 8 that we have available. We considered six different combinations of these to give six different correlation matrices. Our selections are shown in Table I. We note that 48 sweeps tends to be noisy and therefore eliminate it from most of our considerations.

For the 6×6 matrices of $\chi_1 \chi_2$ correlators, a subset of six bases is considered, as shown in Table II corresponding to a choice of 3 smearings to χ_1 and the same 3 for χ_2 . For the 8×8 matrices of $\chi_1 \chi_2$ correlators, a subset of seven bases are considered and are given in Table III corresponding to a choice of 4 smearings to χ_1 and the same 4 for χ_2 . The correlation matrices for χ_1, χ_2 interpolators contain all combinations of correlation functions of χ_1, χ_2 , i.e. $\chi_1 \bar{\chi}_1, \chi_1 \bar{\chi}_2, \chi_2 \bar{\chi}_1$ and $\chi_2 \bar{\chi}_2$.

It is noted that basis operators that are linearly dependent will cause the eigenvalue analysis to fail as there will be a

TABLE I. The bases of 6×6 correlation matrices of $\chi_1 \bar{\chi}_1$.

Sweeps \rightarrow	1	3	7	12	16	26	35	48
Basis No. \downarrow	Bases							
1	1	3	7	12	16	26
2	1	3	7	12	16	...	35	...
3	1	3	7	...	16	26	35	...
4	1	3	...	12	16	26	...	48
5	1	...	7	12	16	26	35	...
6	...	3	7	12	16	26	35	...

TABLE II. The bases of 6×6 correlation matrices of $\chi_1 \chi_2$.

Sweeps \rightarrow	1	3	7	12	16	26	35	48
Basis No. \downarrow	Bases							
1	1	16	48
2	...	3	...	12	...	26
3	...	3	16	48
4	7	...	16	...	35	...
5	12	16	26
6	16	26	35	...

TABLE III. The bases of 8×8 correlation matrices of $\chi_1 \chi_2$.

Sweeps \rightarrow	1	3	7	12	16	26	35	48
Basis No. \downarrow	Bases							
1	1	...	7	...	16	...	35	...
2	7	12	16	26
3	...	3	...	12	...	26	...	48
4	7	12	...	26	35	...
5	7	...	16	26	35	...
6	7	...	16	...	35	48
7	12	16	26	35	...

singularity in the correlation matrix. The fact that our analysis ($\chi_1\bar{\chi}_1$ and $\chi_1\chi_2$) succeeds indicates that our choices of operators access an equal number of dimensions in the Hilbert space. Thus it is interesting to examine the stability of the masses to different choices of bases to ascertain whether one has reliably isolated single eigenstates of QCD. The relevant issues are: (i) whether or not the operators are sufficiently far from collinear that numerical errors do not prevent diagonalization of the correlation matrix and, (ii) whether or not the states of interest have significant overlap with the subspace spanned by our chosen sets of operators. Since our correlation matrix diagonalization succeeded, except at large Euclidean times where statistical errors dominate, we conclude that our operators are sufficiently far from collinear.

IV. RESULTS

A. Variational analysis

We begin by considering the 6×6 correlation matrices of $\chi_1\bar{\chi}_1$ correlators. In Fig. 1, masses from the projected correlation functions and eigenvalues for the 3rd basis of Table I are presented. The basis elements for the 6×6 matrices are highly linearly dependent, and this means the analysis is more complicated than for the 4×4 matrices of Ref. [24]. While the masses from the eigenvalues again display larger dependency on the variational parameters, as observed in Refs. [24,25], masses from the projected correlation functions are very consistent on $t_{\text{start}} (\equiv t)$ and

Δt . Notably, the masses for the ground and first excited states are as robust as in Ref. [24]. For the fifth excited state at the heaviest pion mass with the variational parameters $(t_{\text{start}}, \Delta t) = (6, 1)$, (6,2) and (7,1), (top left graph of Fig. 1), acceptable fits [25] were unobtainable. Nonetheless, the consistency of the calculated masses over the significant sets of variational parameters is self evident, as is how a mass can be exposed using one set of t_{start} and Δt .

From a series of t_{start} and Δt , a single mass is selected for one set of t_{start} and Δt by the selection criteria discussed in Ref. [25], where we prefer a larger value of $t_{\text{start}} + \Delta t$ [27]. In cases where a larger $t_{\text{start}} + \Delta t$ provides a poor signal-to-noise ratio, for example $(t_{\text{start}}, \Delta t) = (7, 3)$ (top left figure), we prefer a little lower $t_{\text{start}} + \Delta t$ value, for example $(t_{\text{start}}, \Delta t) = (7, 2)$, and we follow this procedure for each quark mass.

In Fig. 2, the masses for all the 6×6 correlation matrices of $\chi_1\bar{\chi}_1$ correlators are presented. Straight lines are drawn to illustrate the invariance of the masses over the bases. Since the 1st basis contains all the consecutive smearing sweep counts, i.e. 1, 3, 7, 12, 16, 26 sweeps, it may not span the space as well as other choices. This basis exposes higher first and second excited states and this remains true for the 2nd basis where it contains consecutive five lower smearing sweeps (left figure). These are therefore less reliable bases for extracting excited state masses. It is noted that masses from the third excited state onwards contain higher fluctuations than the lower states,

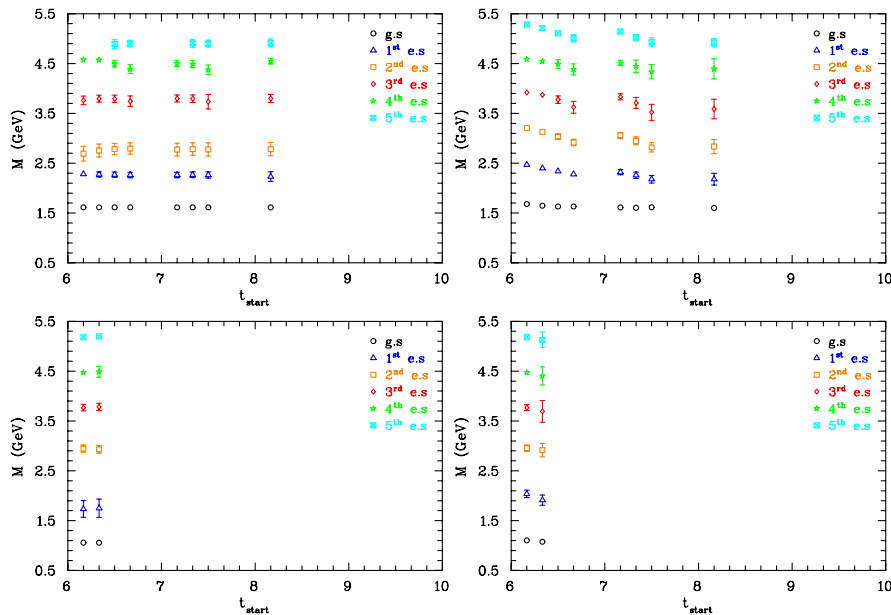


FIG. 1 (color online). Masses of the nucleon, $N^{(1/2)^+}$ states, from the projected correlation functions as shown in Eq. (32) (left) and from the eigenvalues (right) for the 3rd combination (1, 3, 7, 16, 26, 35 sweeps) of 6×6 correlation matrices of $\chi_1\bar{\chi}_1$ correlation functions. The figure corresponds to pion masses of 797 MeV (top row) and 249 MeV (bottom row). Each pair of ground and excited state masses corresponds to the diagonalization of the correlation matrix for each set of variational parameters t_{start} (shown in major tick marks) and Δt (shown in minor tick marks). Here, $t_{\text{start}} \equiv t$, as shown in Eqs. (29) and (31).

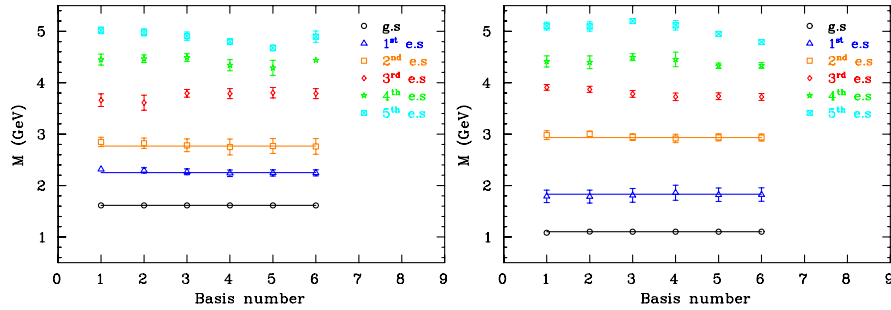


FIG. 2 (color online). Masses of the nucleon, $N^{(1/2)^+}$ states, from the projected correlation functions for the 6×6 correlation matrices of $\chi_1 \bar{\chi}_1$ correlators, for pion masses of 797 MeV (left) and 295 MeV (right). Numbers on the horizontal scale correspond to each basis of 6×6 matrices, for instance, 1 and 2 correspond to the bases of (1, 3, 7, 12, 16, 26 sweeps) and (1, 3, 7, 12, 16, 35 sweeps), respectively, and so on. Masses are extracted according to the selection criteria described in the text and in Ref. [25] from all the combinations of 6×6 correlation matrices as shown in Table I. Straight lines are drawn to illustrate the invariance of the masses over the bases.

independent of the choice of basis. A basis dependence is also evident for the third excited state (right figure). However, the bases from the 3rd to the 6th sets are more consistent, and, in particular, the lower three states are stable over these four bases. Therefore, the bases from 3rd to 6th are used to perform a systematic analysis to calculate the systematic errors associated with the choice of basis, using $\sigma_b = \sqrt{\frac{1}{N_b-1} \sum_{i=1}^{N_b} (M_i - \bar{M})^2}$, where $N_b = 4$ in this case.

In Fig. 3, the final results for the 6×6 correlation matrix analysis of $\chi_1 \bar{\chi}_1$ correlators are shown. As the highest excited state accommodates remaining spectral strength, this state may not be an eigenstate and is not shown in the figure. Masses are averaged over the four bases (from the 3rd to 6th), whereas the errors shown are a combination of average statistical errors ($\bar{\sigma}_s$) over the four bases and systematic errors due to the basis choice (σ_b). As expected

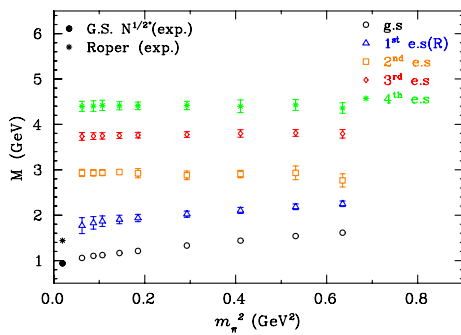


FIG. 3 (color online). Masses of the nucleon, $N^{(1/2)^+}$ states, for the ground (g.s) and the excited (e.s) states from the 6×6 correlation matrices of $\chi_1 \bar{\chi}_1$ correlators over four bases (from the 3rd to the 6th of Fig. 2). The errors shown in the figure are a combination of average statistical errors over these four bases and systematic errors due to basis choices. Errors are combined in quadrature. The black filled symbols are the experimental values of the ground and the Roper states obtained from Ref. [37]. Masses are given in Table IV.

from the 4×4 analysis [24], a similar lower-lying Roper state is also revealed in this 6×6 correlation matrix analysis, which also has a tendency to approach the physical state. This analysis presents six distinct energy states, where the ground and first excited states are extremely robust, emphasizing the utility of the analysis technique presented in Ref. [24]. From this figure it is also evident that the second excited state remains high and an unnatural ordering of the error bars is manifest. Hence there are concerns as to whether this state is a true energy state.

In Ref. [35] addressing negative parity nucleons, a whole new set of nearby states is observed upon introducing χ_2 . Thus, it is important to explore the role of χ_2 in the positive-parity sector. In Fig. 4, masses from the projected correlation functions and eigenvalues for the 6×6 correlation matrix analysis of $\chi_1 \chi_2$ correlators are presented. The diagonalization is only successful for the heavier four quarks, which again proves that a variational analysis with χ_2 interpolator is always a challenge [25]. This interpolator vanishes in the nonrelativistic limit [8,36] and is renowned for providing noisier correlation functions [11,12] especially for the lighter quark masses, where one otherwise might expect the relativistic nature of the quarks to be of benefit. The Euclidean-time correlation functions of the χ_2 interpolator decay more rapidly, and the signal-to-noise ratio also deteriorates more quickly with time. In Refs. [24,25], a rise from below of excited state masses from the projected correlation functions was observed for the linearly dependent operators. This is also manifest in the 6×6 analysis of $\chi_1 \bar{\chi}_1$, shown in Fig. 1, but for the 6×6 analysis of $\chi_1 \chi_2$ correlators, these effects are reduced. This is expected because the basis elements of these bases are likely to be more orthogonal, improving the isolation of states.

In Fig. 5, projected masses from all the 6×6 correlation matrices of $\chi_1 \chi_2$ are presented. Again the ground state is robust in this analysis. As the 6th combination contains a consecutively higher number of smearing sweeps

TABLE IV. Masses of the nucleon, $N^{(1/2)^+}$ states, averaged over the four bases (from the 3rd to 6th). The errors shown here are a combination of average statistical errors over four bases and systematic errors for the choice of basis, combined in quadrature.

aM_π	$aM_{g.s.}$	$aM_{1^{st}e.s.}$ (Roper)	$aM_{2^{nd}e.s.}$	$aM_{3^{rd}e.s.}$	$aM_{4^{th}e.s.}$
0.5141(19)	1.0414(68)	1.451(40)	1.784(93)	2.447(60)	2.813(76)
0.4705(20)	0.9933(78)	1.409(41)	1.892(98)	2.459(49)	2.856(78)
0.4134(22)	0.9286(80)	1.357(43)	1.875(54)	2.451(54)	2.838(90)
0.3490(24)	0.8588(88)	1.305(45)	1.857(61)	2.436(41)	2.849(59)
0.2776(24)	0.781(10)	1.250(53)	1.886(65)	2.427(39)	2.845(54)
0.2452(24)	0.752(11)	1.229(60)	1.903(38)	2.423(42)	2.846(58)
0.2110(27)	0.722(14)	1.204(75)	1.894(42)	2.417(45)	2.850(72)
0.1905(31)	0.711(12)	1.180(89)	1.892(46)	2.414(47)	2.840(74)
0.1607(35)	0.682(14)	1.142(11)	1.891(51)	2.410(55)	2.837(72)

(16, 26, 35), this basis is not as reliable as the other sets. The first excited state extracted with this basis sits somewhat lower than the other five bases. A careful analysis of Figs. 5 and 2 reveals that in the vicinity of the second excited state from the 6×6 analysis of $\chi_1 \bar{\chi}_1$ correlators (Fig. 2), three excited states appear in the 6×6 analysis of $\chi_1 \chi_2$ (Fig. 5). A completely new excited state, the second

excited state, is extracted in the $\chi_1 \chi_2$ analysis. This second excited state is robust for all bases (left figure). The signal-to-noise ratio for this state deteriorates more rapidly for the light quark (right figure). Interestingly, the fifth excited state extracted from the $\chi_1 \chi_2$ matrices sits at a significantly lower energy state than those from the $\chi_1 \bar{\chi}_1$ matrices, reflecting the fact that two new low-lying states have

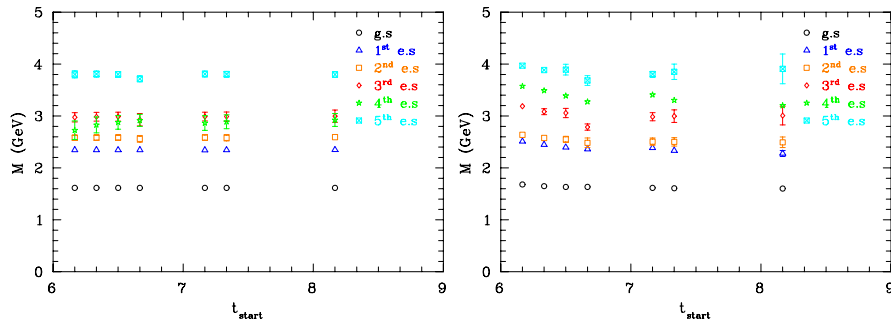


FIG. 4 (color online). Masses of the nucleon, $N^{(1/2)^+}$ states, from the projected correlation functions as shown in Eq. (32) (left) and from the eigenvalues (right) for the 3rd combination (3, 16, 48 sweeps) of 6×6 correlation matrices of $\chi_1 \chi_2$ correlation functions. The figure corresponds to the pion mass of 797 MeV. Each pair of ground and excited states mass corresponds to the diagonalization of the correlation matrix for each set of variational parameters t_{start} (shown in major tick marks) and Δt (shown in minor tick marks).

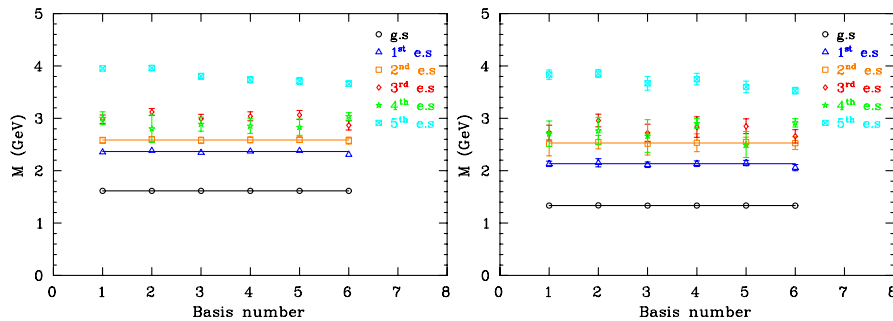


FIG. 5 (color online). Masses of the nucleon, $N^{(1/2)^+}$ states, from the projected correlation functions for the 6×6 correlation matrices of $\chi_1 \chi_2$ correlators, for pion masses of 797 MeV (left) and 541 MeV (right). Numbers on the horizontal scale correspond to each basis of 6×6 matrices, for instance, 1 and 2 correspond to the bases of (1, 16, 48 sweeps) and (3, 12, 26 sweeps), respectively, and so on. Masses are extracted according to the selection criteria described in the text and in Ref. [25] from all the combinations of 6×6 matrices as shown in Table II. Straight lines are drawn to illustrate the invariance of the masses over the bases.

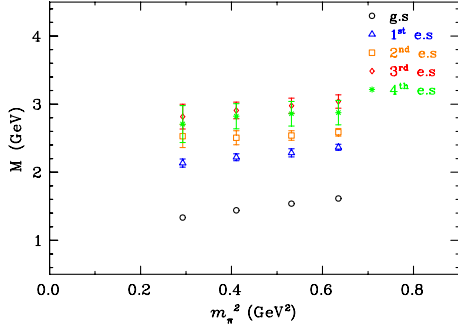


FIG. 6 (color online). Masses of the nucleon, $N^{(1/2)^+}$ states, for the ground (g.s) and the excited (e.s) states from the 6×6 correlation matrices of $\chi_1 \chi_2$ correlators over five bases (from the 1st to 5th of Fig. 5). The errors shown in the figure are a combination of average statistical errors over these five bases and systematic errors due to basis choices. Errors are combined in quadrature. Masses are given in Table V.

been revealed. The third and fourth excited states are nearly degenerate in this analysis. As the results for the lower three states are consistent over five basis choices (from 1st to 5th) of the 6×6 matrices, we perform a systematic analysis over these five bases, as discussed previously.

In Fig. 6, a summary of the 6×6 correlation matrix analysis of $\chi_1 \chi_2$ correlators is presented. Masses are averaged over the five bases, while errors are a combination of average statistical and systematic errors due to basis choices. Apart from the ground and the first excited states, this analysis presents a distinct second excited state for the three heavier quark masses. The signal for the light quark mass for this state is poor. This analysis reveals new nearly degenerate third and fourth excited states, that the 6×6 bases of $\chi_1 \bar{\chi}_1$ correlation functions are unable to resolve.

In Fig. 7, masses from the projected correlation functions and eigenvalues for the 8×8 correlation matrix of $\chi_1 \chi_2$ correlators are presented. Similar to the 6×6 analysis of $\chi_1 \chi_2$, this analysis is also successful for the heavier four quark masses. The enhanced dimension of the matrices means the numerical diagonalization is less stable, and so the variational analysis is only successful for a few sets of variational parameters, t_{start} and Δt . However, in Fig. 7,

there is sufficient consistency between the masses from the projected correlation functions for each set of t_{start} and Δt . As before, the 8×8 analysis gives a projected mass which is highly independent of the variational parameters. Here we have selected $t_{\text{start}} = 6$, $\Delta t = 2$.

In Fig. 8, masses from the projected correlation functions for all combinations of 8×8 correlation matrices are shown. All the bases reveal a very consistent ground state mass. A systematic basis dependency of the excited states (from third excited state onwards) is noticed for the 1st and 2nd combinations. As the 1st combination consists of 1 and 7 smearing sweeps, it provides a higher mass from the third excited state onwards, in comparison with the other bases. The 2nd basis contains consecutive smearing sweep counts, starting with 7 sweeps, and ending with a moderate sweep count of 26. This provides less diversity in this basis for the higher excited states and also provides a higher mass from the third excited state onwards. Therefore, the 1st and 2nd bases are not as reliable as other sets. The fifth and sixth excited states sit a little high for the 7th basis which has a narrow cluster of smearing sweeps and is therefore likely to be less reliable in spanning the space. Bases from the 3rd to 6th sets have more smearing diversity being well spread over the range of smearing sweep counts starting from 3 and 7 sweeps. It is also evident from Fig. 8 that the 3rd to 6th combinations of smearing sweeps are successful in providing highly consistent lower energy states. As before, we will therefore perform a systematic analysis over these four bases. It is interesting to note that in the vicinity of the fifth excited state from the 6×6 analysis of $\chi_1 \chi_2$, the 8×8 correlation matrix presents three excited states.

In Fig. 9, a summary of the 8×8 correlation matrix results are presented. As in Fig. 6, a distinct second excited state is also obtained in this 8×8 analysis, for the two heavier quark masses. However, increased separation of the third and fourth excited states appears here with the enlarged basis. A careful examination reveals that the first excited state extracted in this analysis is a little lower than in the 6×6 analysis of $\chi_1 \chi_2$ (see Fig. 6). In accord with the principle of the variational method, our analysis signifies the importance of using larger correlation matrices to reliably isolate the higher energy eigenstates of QCD.

TABLE V. Masses of the nucleon, $N^{(1/2)^+}$ states, averaged over the five bases (from the 1st to 5th). The errors shown here are a combination of average statistical errors over these bases and systematic errors for the choice of basis, combined in quadrature.

aM_π	$aM_{g.s}$	$aM_{1^{\text{st}}e.s}(\text{Roper})$	$aM_{2^{\text{nd}}e.s}$	$aM_{3^{\text{rd}}e.s}$	$aM_{4^{\text{th}}e.s}$
0.5141(19)	1.0419(65)	1.526(28)	1.669(37)	1.960(64)	1.85(12)
0.4705(20)	0.9927(69)	1.474(39)	1.638(45)	1.920(72)	1.84(12)
0.4134(22)	0.9295(75)	1.432(33)	1.617(66)	1.875(79)	1.82(12)
0.3490(24)	0.8612(84)	1.377(39)	1.63(11)	1.81(12)	1.74(17)

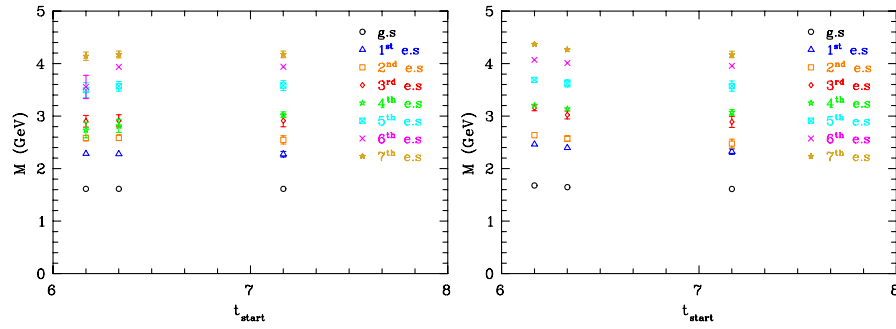


FIG. 7 (color online). Masses of the nucleon, $N^{(1/2)^+}$ states, from the projected correlation functions as shown in Eq. (32) (left) and from the eigenvalues (right) for the 3rd combination (3, 16, 48 sweeps) of 8×8 correlation matrices of $\chi_1 \chi_2$ correlation functions. The figure corresponds to the pion mass of 797 MeV. Each pair of ground and excited states mass corresponds to the diagonalization of the correlation matrix for each set of variational parameters t_{start} (shown in major tick marks) and Δt (shown in minor tick marks).

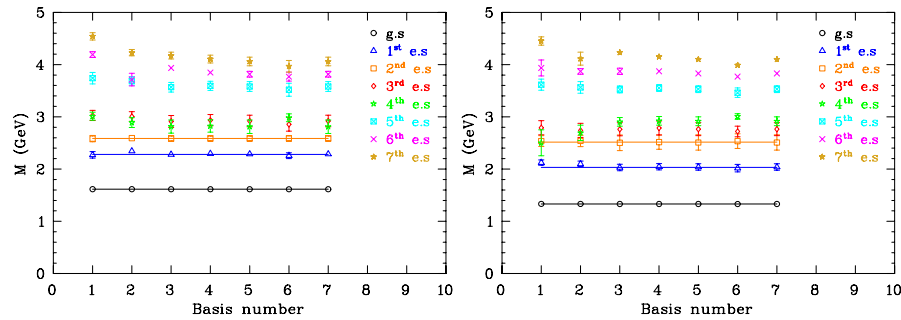


FIG. 8 (color online). Masses of the nucleon, $N^{(1/2)^+}$ states, from the projected correlation functions for the 8×8 correlation matrices of $\chi_1 \bar{\chi}_2$ correlators, for pion masses of 797 MeV (left) and 541 MeV (right). Numbers on the horizontal scale correspond to each basis of 8×8 matrices, for instance, 1 and 2 correspond to the bases of (1, 7, 16, 35 sweeps) and (7, 12, 16, 26 sweeps), respectively, and so on. Masses are extracted according to the selection criteria described in the text and in Ref. [25] from all the combinations of 8×8 matrices as shown in Table III. Straight lines are drawn to illustrate the invariance of the masses over the bases.

B. Splitting of excited states

In Fig. 10, we show how the excited energy states depend on the choice of correlation functions and the dimension of the correlation matrix. The ground state is

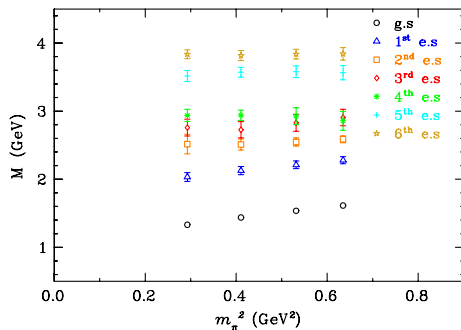


FIG. 9 (color online). Masses of the nucleon, $N^{(1/2)^+}$ states, for the ground (g.s.) and the excited (e.s.) states from the 8×8 correlation matrices of $\chi_1 \bar{\chi}_2$ correlators over four bases (from the 3rd to 6th of Fig. 8). The errors shown in the figure are a combination of average statistical errors over these four bases and systematic errors due to basis choices, combined in quadrature. Masses are given in Table VI.

clearly independent of the dimension of the matrices and choice of interpolating fields. The excited state extracted from the 2×2 correlation matrix splits into two excited states with the 3×3 matrix. The central value of the first excited state, extracted with the 3×3 matrix, is a little lower than that of the 2×2 case. Interestingly, the second excited state from the 3×3 matrix is in very good agreement with the excited state number of the 2×2 analysis.

The 4×4 analysis of $\chi_1 \bar{\chi}_1$ correlation functions reveals a lower first excited state (Roper state) [24] and two other heavier excited states. Therefore, the 4×4 basis of $\chi_1 \bar{\chi}_1$ correlation functions is able to resolve and isolate the superposition of eigenstates in the 3×3 matrix. The 6×6 and 4×4 correlation matrices of $\chi_1 \bar{\chi}_1$ correlators provide very consistent results for the lower four energy states, and the 6×6 analysis is able to extract two new higher energy states. The larger error bar of the third (highest) excited state extracted with the 4×4 correlation matrix compared to the 6×6 result of $\chi_1 \bar{\chi}_1$ is a manifestation of accommodating remaining spectral strength in this (third excited) state in the 4×4 analysis and hence is unreliable [24].

TABLE VI. Masses of the nucleon, $N^{(1/2)^+}$ states, averaged over four bases (from the 3rd to 6th). The errors shown here are a combination of average statistical errors over these four bases and systematic errors for the choice of basis, combined in quadrature.

aM_π	$aM_{g,s}$	$aM_{1^{st}e.s}(R)$	$aM_{2^{nd}e.s}$	$aM_{3^{rd}e.s}$	$aM_{4^{th}e.s}$	$aM_{5^{th}e.s}$	$aM_{6^{th}e.s}$
0.5141(19)	1.0412(66)	1.470(33)	1.669(33)	1.874(78)	1.843(90)	2.300(67)	2.478(58)
0.4705(20)	0.9912(71)	1.427(35)	1.642(38)	1.825(79)	1.888(80)	2.309(54)	2.475(46)
0.4134(22)	0.9277(77)	1.372(38)	1.619(52)	1.758(77)	1.896(48)	2.304(45)	2.462(47)
0.3490(24)	0.8588(86)	1.311(42)	1.623(92)	1.779(80)	1.895(57)	2.269(52)	2.475(41)

The 6×6 analysis of $\chi_1\chi_2$ correlation functions extracts different excited states than those of the 6×6 analysis of $\chi_1\bar{\chi}_1$ alone. The first excited state extracted with this basis sits high in comparison with the Roper state. Thus, a basis of four different smearings with $\chi_1\bar{\chi}_1$ is essential to isolating the single eigenstate associated with the Roper resonance. Another interesting feature is the splitting of the ‘‘second excited state’’ of the $\chi_1\bar{\chi}_1$ analysis into three nearby states with the new χ_2 spin-flavor combinations.

The final very interesting outcomes are revealed from the 8×8 correlation matrix analysis of $\chi_1\chi_2$. This analysis provides a first excited state which is in excellent agreement with the Roper state revealed by $\chi_1\bar{\chi}_1$ correlators alone. This present investigation reveals that χ_2 plays a subtle role for the Roper. We note however that a new nearby second excited state is revealed in the $\chi_1\chi_2$ analysis and a future high-statistics analysis may reveal it is essential to resolve this state correctly to obtain the first excited state accurately. This basis also provides second, third and fourth excited states consistent with the 6×6 analysis of $\chi_1\chi_2$. However, the fifth excited state coming from this analysis is a little lower than that of the 6×6 matrix of $\chi_1\chi_2$. There the fifth state accommodates all remaining

spectral strength. This state wasn’t identified in the $\chi_1\bar{\chi}_1$ analysis. The sixth excited state provided by this analysis is consistent with the third excited state extracted with the 6×6 analysis of $\chi_1\bar{\chi}_1$. It is worth noting that the basis of $\chi_1\bar{\chi}_1$ correlation functions is insufficient to isolate the second excited state of the nucleon.

While this analysis is able to provide some evidence that the first five energy-states are reasonably robust through comparisons of 6×6 and 8×8 , only a more comprehensive higher dimension correlation matrix analysis can assess the reliability of the sixth and seventh states.

In Fig. 11, a summary of results for the positive-parity excited states of the nucleon is presented. In Ref. [37], the quality of the P_{11} (1710) MeV state is characterized by three stars (***) and P_{11} (2100 MeV) state by one star (*). These resonance states decay through the $N \rightarrow N\pi\pi$ channel with positive parity. Therefore, looking at both the S-wave $N + \pi + \pi$ and P-wave $N + \pi$ decay channels provides information related to these resonances. The second excited state is very close to the threshold $N + \pi$ state but has a different slope. It is also evident that this state is significantly different and lower than the $N + \pi + \pi$ state for the heavier three quark masses providing evidence

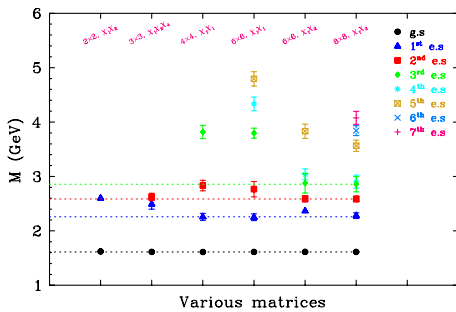


FIG. 10 (color online). Masses of the nucleon, $N^{(1/2)^+}$ states, for the various dimensions of correlation matrices, as labeled on the upper horizontal axis. The 2×2 and 3×3 results for the smeared-smeared correlation functions with 26 sweeps of smearing are taken from Ref. [25], while the 4×4 results are from Ref. [24]. The 6×6 and 8×8 results correspond to the analyses presented in this paper. Dotted lines are drawn to aid in illustrating the consistency of the results. Figure corresponds to the pion mass of 797 MeV.

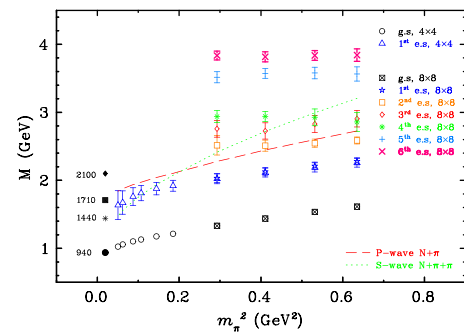


FIG. 11 (color online). Masses of the nucleon, $N^{(1/2)^+}$ states, from the 8×8 correlation matrices of $\chi_1\chi_2$, and 4×4 correlation matrices of $\chi_1\bar{\chi}_1$ as a function of the squared pion mass, for the ground (g.s.), first through sixth excited states (e.s.). The experimental values are taken from Ref. [37], where the reliability of the ground and Roper states are signified by four stars (****), P_{11} (1710) MeV state by three stars (***) and P_{11} (2100 MeV) state by one star (*).

that this state is best described as a single particle state. It is also noted that the third and fourth excited states have a mass dependence different from the multiparticle states. This suggests that these two energy states revealed here are more likely to be single particle resonance states. Simulations on larger lattice volumes and at lighter quark masses are necessary to resolve this issue.

Figure 12 provides a comparison of the nucleon spectrum revealed in this comprehensive analysis with state-of-the-art results from Refs. [17,38] in quenched QCD. The results from the BGR Collaboration [38] follow from an analysis similar to ours where fermion source smearing is key to providing a basis which enables the isolation of excited states. However, they use only two levels of source smearing and use different smearings for each quark flavor within a given interpolator. The fact that their Roper state sits high relative to our result is consistent with our observation that a minimum of four different smearing levels is required to obtain a stable low-lying state. Whereas our 6×6 analysis with six different smearing levels did not change the mass of the Roper state from our 4×4 analysis, the consideration of only three smearing levels did lead to a higher mass Roper state.

Results from the LHP Collaboration [17] are illustrated at $m_\pi = 490$ MeV. Here we have reported all states that may have spin-1/2 quantum numbers. The Roper state in their analysis sits higher than both the present analysis and the results of Ref. [38]. As their scale determination provides a low nucleon mass, the excited state masses will become higher again if one sets the scale to reproduce the nucleon mass of this analysis or that of Ref. [38]. It suggests that their consideration of a single level of source smearing may be insufficient to provide a basis suitable to resolve the Roper state. Our expectation is that the introduction of a variety of source smearings into their basis operators may be beneficial. It would be interesting to expand their basis to include several levels of source

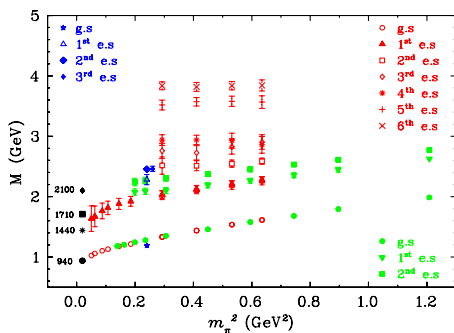


FIG. 12 (color online). Masses of low-lying nucleon states from this work (legend at top right), from Ref. [17] (legend at top left) and Ref. [38] (legend at bottom right). The results from Ref. [17] correspond to $m_\pi = 490$ MeV, where the nearly degenerate fourth energy state has been shifted a little to the right for clarity.

smearing to explore the extent to which the excited state masses change.

V. CONCLUSIONS

In this paper, we have presented a comprehensive correlation matrix analysis of the positive-parity spin- $\frac{1}{2}$ excitations of the nucleon. We have considered large dimensions of correlation matrices, built from smeared-smeared correlation functions of $\chi_1 \bar{\chi}_1$ and $\chi_1 \chi_2$ correlators. The results of this paper, for the ground and Roper states of the nucleon, are very consistent with the discovery of the Roper in Ref. [24] from a 4×4 correlation matrix of $\chi_1 \bar{\chi}_1$ alone. Thus, the most important conclusion is that the earlier first result for the Roper [24] is robust under the comprehensive analysis presented herein.

This paper signifies the importance of using a variety of smearings in making an operator basis and the importance of comparing the results across a range of choices of basis for the correlation matrix. In particular, it emphasizes the use of at least four different smearing levels to isolate the elusive Roper state.

In addition, we have reported new second, third, fourth, fifth and sixth excited-states of the nucleon. While both the $\chi_1 \bar{\chi}_1$ and $\chi_1 \chi_2$ correlation matrices provide excellent agreement for the ground and the Roper states, only the $\chi_1 \chi_2$ analysis provides access to a completely new (second) excited eigenstate. All the correlation matrix analyses provide a very consistent third excited state, see Fig. 10. Simulations on larger lattice volumes at lighter quark masses with higher statistics will be interesting to investigate the propagation of these states towards light quark masses.

Another interesting result of this paper is delineating the nature of the splitting of the excited states of the nucleon, as seen in Fig. 10, for the variational method. While the ground state is independent of any basis choice, and the dimension of the matrix used, extracting a particular excited state can depend on the interpolators making the correlation functions. For example, a variational analysis of $\chi_1 \bar{\chi}_1$ correlation functions does not provide the second excited state, indicating that the χ_1 interpolator either does not couple or only has a very small coupling to this state. We emphasize the importance of using a large correlation matrix for a reliable extraction of excited states' energies.

Because of the difficulties in ascertaining that a given set of basis interpolators is sufficient to isolate all the eigenstates of QCD in the mass range of interest, we believe that it is essential to resolve the nucleon spectrum using a wide variety of approaches. For example, it is now apparent that the consideration of a single level of fermion source smearing is unlikely to be sufficient to resolve the low-lying Roper state. Future investigations should explore the role of fermion source smearing in providing a suite

of basis operators that span the space in an effective manner.

To test the robustness of the spectrum revealed in this analysis it will be important for future studies to carefully examine a wide variety of different interpolators in order to test whether or not other low-lying states will appear in the spectrum. For example, we anticipate that five-quark operators will be essential in accessing the relevant low-lying meson-baryon scattering states.

ACKNOWLEDGMENTS

This research was undertaken on the NCI National Facility in Canberra, Australia, which is supported by the Australian Commonwealth Government. We also acknowledge eResearch SA for generous grants of supercomputing time which have enabled this project. This research is supported by the Australian Research Council.

-
- [1] N. Isgur and G. Karl, *Phys. Lett. B* **72**, 109 (1977).
 - [2] N. Isgur and G. Karl, *Phys. Rev. D* **19**, 2653 (1979).
 - [3] Z.-p. Li, V. Burkert, and Z.-j. Li, *Phys. Rev. D* **46**, 70 (1992).
 - [4] C. E. Carlson and N. C. Mukhopadhyay, *Phys. Rev. Lett.* **67**, 3745 (1991).
 - [5] P. A. M. Guichon, *Phys. Lett. B* **164**, 361 (1985).
 - [6] O. Krehl, C. Hanhart, S. Krewald, and J. Speth, *Phys. Rev. C* **62**, 025207 (2000).
 - [7] S. Durr *et al.*, *Science* **322**, 1224 (2008).
 - [8] D. B. Leinweber, *Phys. Rev. D* **51**, 6383 (1995).
 - [9] F. X. Lee and D. B. Leinweber, *Nucl. Phys. B, Proc. Suppl.* **73**, 258 (1999).
 - [10] M. Gockeler *et al.* (QCDSF), *Phys. Lett. B* **532**, 63 (2002).
 - [11] S. Sasaki, T. Blum, and S. Ohta, *Phys. Rev. D* **65**, 074503 (2002).
 - [12] W. Melnitchouk *et al.*, *Phys. Rev. D* **67**, 114506 (2003).
 - [13] R. G. Edwards, U. M. Heller, and D. G. Richards (LHP), *Nucl. Phys. B, Proc. Suppl.* **119**, 305 (2003).
 - [14] F. X. Lee *et al.*, *Nucl. Phys. B, Proc. Suppl.* **119**, 296 (2003).
 - [15] N. Mathur *et al.*, *Phys. Lett. B* **605**, 137 (2005).
 - [16] S. Sasaki, *Prog. Theor. Phys. Suppl.* **151**, 143 (2003).
 - [17] S. Basak *et al.*, *Phys. Rev. D* **76**, 074504 (2007).
 - [18] J. M. Bulava *et al.*, *Phys. Rev. D* **79**, 034505 (2009).
 - [19] J. Bulava *et al.*, *Phys. Rev. D* **82**, 014507 (2010).
 - [20] G. P. Engel, C. B. Lang, M. Limmer, D. Mohler, and A. Schafer (BGR [Bern-Graz-Regensburg]), *Phys. Rev. D* **82**, 034505 (2010).
 - [21] K. Sasaki, S. Sasaki, and T. Hatsuda, *Phys. Lett. B* **623**, 208 (2005).
 - [22] C. Michael, *Nucl. Phys.* **B259**, 58 (1985).
 - [23] M. Luscher and U. Wolff, *Nucl. Phys.* **B339**, 222 (1990).
 - [24] M. S. Mahbub *et al.*, *Phys. Lett. B* **679**, 418 (2009).
 - [25] M. S. Mahbub *et al.*, *Phys. Rev. D* **80**, 054507 (2009).
 - [26] S. Gusken, *Nucl. Phys. B, Proc. Suppl.* **17**, 361 (1990).
 - [27] B. Blossier, M. Della Morte, G. von Hippel, T. Mendes, and R. Sommer, *J. High Energy Phys.* 04 (2009) 094.
 - [28] T. Takaishi, *Phys. Rev. D* **54**, 1050 (1996).
 - [29] P. de Forcrand *et al.* (QCD-TARO), *Nucl. Phys.* **B577**, 263 (2000).
 - [30] J. M. Zanotti *et al.* (CSSM Lattice), *Phys. Rev. D* **65**, 074507 (2002).
 - [31] J. M. Zanotti, B. Lasscock, D. B. Leinweber, and A. G. Williams, *Phys. Rev. D* **71**, 034510 (2005).
 - [32] R. Sommer, *Nucl. Phys.* **B411**, 839 (1994).
 - [33] C. Morningstar and M. J. Peardon, *Phys. Rev. D* **69**, 054501 (2004).
 - [34] B. G. Lasscock *et al.*, *Phys. Rev. D* **72**, 074507 (2005).
 - [35] M. S. Mahbub, W. Kamleh, D. B. Leinweber, A. O. Cais, and A. G. Williams, *Phys. Lett. B* **693**, 351 (2010).
 - [36] D. B. Leinweber, R. M. Woloshyn, and T. Draper, *Phys. Rev. D* **43**, 1659 (1991).
 - [37] C. Amsler *et al.* (Particle Data Group), *Phys. Lett. B* **667**, 1 (2008).
 - [38] T. Burch *et al.*, *Phys. Rev. D* **74**, 014504 (2006).